Performance Impacts of Practical Fabrication Tradeoffs for a Radial Flux Coaxial Magnetic Gear with Halbach Arrays and Air Cores

Matthew C. Gardner
Elec. and Comp. Engr.
Texas A&M University
College Station, TX, USA
gardner1100@tamu.edu

Matthew Johnson
Army Research Lab
U. S. Army CCDC
College Station, TX, USA
matthew.c.johnson186.civ@mail.mil

Hamid A. Toliyat
Elec. and Comp. Engr.
Texas A&M University
College Station, TX, USA
toliyat@tamu.edu

***Abstract*—This paper evaluates the impacts of various means of securing the magnetically active materials in a radial flux coaxial magnetic gear with Halbach arrays and air cores. Rods through holes in the modulators and spacers between adjacent modulators can be used to attach the modulators to their end caps with a minimal reduction of the design's slip torque. A bridge between adjacent modulators simplifies assembly but significantly reduces the slip torque. Retention sleeves can secure the magnets, but, due to an increase in the effective air gaps, these sleeves drastically reduce the slip torque, especially if the effective outer air gap is increased. Nonmagnetic walls between adjacent magnets facilitate positioning and holding the magnets but significantly reduce the slip torque. However, extending the magnets axially beyond the modulators provides additional space for structural support while increasing the slip torque. A prototype with a 4.67:1 gear ratio was fabricated and tested. Its active material torque density of 25.2 N·m/kg is competitive with commercially available mechanical planetary gear examples. However, when the structural mass of the prototype is considered, its torque density is 7.1 N·m/kg. It achieves 99% efficiency, which is higher than the efficiency of the example mechanical gears.**

Keywords—air core, coreless, efficiency, gear, Halbach, light weight, magnetic gear, specific torque, torque density

I. Introduction

Magnetic gears perform the same function as mechanical gears, transforming power between low-speed, high-torque rotation and high-speed, low-torque rotation. However, unlike mechanical gears, magnetic gears rely on modulated magnetic fields instead of physically interlocking teeth [1]-[3]. This noncontact operation results in a plethora of potential benefits, including improved reliability, reduced maintenance, and reduced acoustic noise. Thus, magnetic gears have attracted significant interest for a wide variety of applications, from wind [4] and wave [5], [6] energy harvesting to electric vehicles [7] and aerospace platforms [8], [9].

Fig. 1(a) shows the magnetically active portions of a conventional radial flux coaxial magnetic gear with surface permanent magnets (SPMs). The gear consists of three rotors: an inner low pole count rotor (Rotor 1), an intermediate rotor comprised of ferromagnetic pieces (known as "modulators") separated by nonmagnetic slots (Rotor 2), and an outer high pole count rotor (Rotor 3). Usually, Rotor 1 is the high speed rotor and Rotor 2 or Rotor 3 is the low speed rotor, with the other rotor being fixed in place.

Halbach arrays have previously been applied to magnetic gears to increase torque density, improve efficiency, and reduce torque ripple [10]-[13]. Additionally, because Halbach arrays concentrate flux on one side of the array and reduce it on the other side, gears with Halbach arrays may achieve high torque densities without back irons [11]. Replacing the back irons with a lighter nonmagnetic material, such as plastic, can significantly reduce a design's mass. Because the nonmagnetic material has similar magnetic properties to air, such a design is described as having an "air core." Fig. 1(b) illustrates the magnetically active portions of an example radial flux magnetic gear with Halbach arrays and air cores on both rotors. As minimizing mass is critical for aerospace applications, NASA has developed two prototypes with Halbach arrays [8].

Magnetic gears present several fabrication challenges. First, the modulators must be supported between the two sets of permanent magnets (PMs). These PMs create strong magnetic forces, which can cause the modulators to bend into the air gaps [14]. Additionally, the PMs' rotating flux harmonics can induce

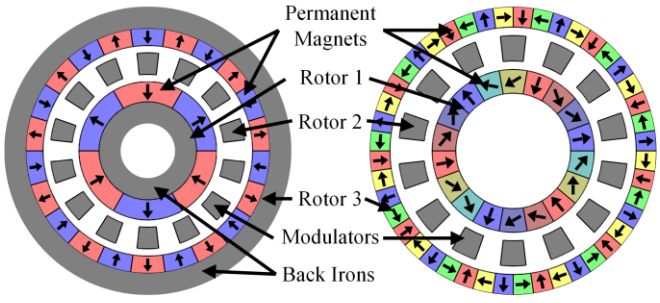

Fig. 1. Magnetically active portions of (a) a conventional radial flux coaxial magnetic gear with surface PMs and (b) a radial flux coaxial magnetic gear with Halbach arrays and air cores.

Research was sponsored by the Army Research Laboratory and was accomplished under Cooperative Agreement Number W911NF-18-2-0289. The views and conclusions contained in this document are those of the authors and should not be interpreted as representing the official policies, either expressed or implied, of the Army Research Laboratory or the U.S. Government. The U.S. Government is authorized to reproduce and distribute reprints for Government purposes notwithstanding any copyright notation herein.

eddy currents in any conductive materials in this region, so the modulators should be laminated or made of soft magnetic composites, instead of solid steel pieces, to improve efficiency, especially at higher speeds [9]. Second, while conventional machines only have two concentric bodies separated by one air gap, a coaxial magnetic gear has three concentric bodies separated by two air gaps. Third, as in conventional SPM machines, the permanent magnets must be retained on both Rotor 1 and Rotor 3. It is especially important to retain the Rotor 1 PMs at high speeds.

The use of Halbach arrays and air cores increases the complexity of fabricating a magnetic gear. First, there are strong magnetic forces on each of the pieces in a discrete Halbach array, which makes assembly and PM retention more challenging. This is exacerbated by the fact that the PMs do not experience any magnetic attraction to the air cores (as they would to back irons). Thus, for the prototype described in [15], back irons were added to simplify holding the PMs, even though this reduced the torque density. Additionally, due to the lack of magnetic containment provided by the back irons, the flux from Rotor 1 may extend beyond Rotor 3 [16]. This may cause losses in nearby conductive objects and attract nearby magnetic objects. Also, the use of plastic instead of steel can exacerbate thermal challenges, such as removing heat from eddy currents in the PMs and stresses from uneven thermal expansion. This paper systematically addresses the impacts of various tradeoffs involved in solving some of these fabrication challenges for an example design described in Table I and Fig. 2. This base design operates with Rotor 1 as the high speed rotor, Rotor 2 as the low speed rotor, and Rotor 3 fixed, which results in a 4.67:1 gear ratio. The PMs are NdFeB N52, and the modulators are made of 26 gauge M19 laminations. All simulation sweep results in this paper were produced by sweeping only one or two of the base design parameters from their base values at a time.

TABLE I. PROTOTYPE DESIGN PARAMETER VALUES

Symbol	Description	Values
P_1	Number of Rotor 1 pole pairs	3
Q_2	Number of modulators	14
P_3	Number of Rotor 3 pole pairs	11
N_1	Number of PM pieces per Rotor 1 pole	2
N_3	Number of PM pieces per Rotor 3 pole	2
R_{Out}	Outer radius of Rotor 3 PMs	50.8 mm
T_{PM3}	Radial thickness of Rotor 3 PMs	5 mm
T_{OAG}	Outer air gap thickness	1 mm
T_{Mods}	Radial thickness of Rotor 2	7.5 mm
T_{Bridge}	Radial thickness of modulator bridge	1.5 mm
T_{IAG}	Effective inner magnetic air gap thickness	2.5 mm
T_{PM1}	Radial thickness of Rotor 1 PMs	8 mm
$w_{R3,Out}$	Tangential width between Rotor 3 PMs at their outer radius	1.5 mm
$w_{R3,In}$	Tangential width between Rotor 3 PMs at their inner radius	2 mm
w_{R1}	Tangential width between Rotor 1 PMs	1.5 mm
$\alpha_{Mods,Out}$	Modulators fill factor at the Rotor 2 outer radius	0.5
$\alpha_{Mods,In}$	Modulators fill factor at the Rotor 2 inner radius	0.7
R_{Hole}	Radius of modulator holes	1.2 mm
L_{PM3}	Axial length of Rotor 3 PMs	51.8 mm
L_{Mods}	Axial length of modulators	37.8 mm
L_{PM1}	Axial length of Rotor 1 PMs	47.8 mm

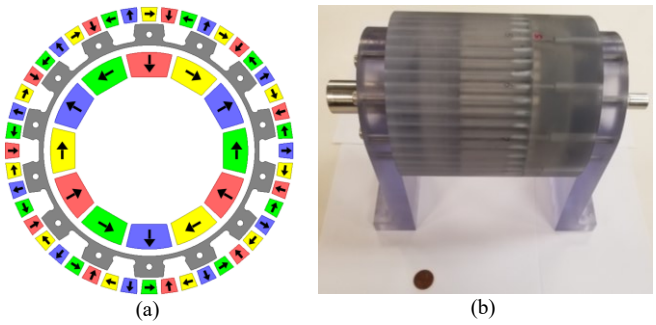

(a) (b)

Fig. 2. (a) Magnetically active portion of the base design and (b) assembled prototype with a penny for a size reference.

II. MODULATORS SUPPORT

To simplify handling and fabrication, the modulator stack was bonded. However, additional modulator support is required. One means of support used in this prototype is to place rods through the axial length of the modulators, as in [5], [6]. For this design, these rods are made of G10 fiberglass-epoxy laminate to provide high strength with high electrical resistivity. Additionally, the slots between adjacent modulators are filled with glass-filled nylon spacers. Circular arc shaped holes are cut out of the modulators' inner corners to allow the spacers to interlock well with the modulators. Both the circular holes for the rods and the arc shaped holes remove magnetically permeable material from the flux paths in the modulators, as depicted in Fig. 2(a). Fig. 3 illustrates how the radii of these holes impact the design's slip torque and full load electromagnetic efficiency at the rated Rotor 2 speed of 400 rpm based on finite element analysis (FEA). Generally, these holes do not have much effect on the performance unless they become large enough that the area between them is thoroughly saturated, worsening gear performance. For this design, the holes have radii of 1.2 mm. Fig. 3(b) also indicates that this design has a very high electromagnetic efficiency (neglecting mechanical losses), which mitigates thermal concerns. A few factors contribute to this high electromagnetic efficiency. First, a Halbach array produces more sinusoidal fields than a conventional SPM configuration, which reduces both torque ripple and losses due to unwanted harmonics. Second, the PMs are segmented into multiple pieces per pole to form the discrete

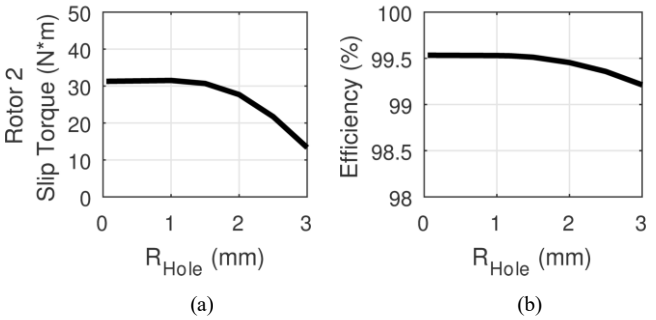

(a) (b)

Fig. 3. Impact of modulator holes radii (varied together) on (a) Rotor 2 slip torque, based on 3D FEA, and (b) electromagnetic efficiency at rated speed and maximum torque, based on 2D FEA.

Halbach arrays, which reduces eddy current losses. Third, the air core design eliminates core losses in the back irons because it eliminates the back irons themselves.

Another way to support the modulators is to connect adjacent modulators with one or more thin bridges [5], [6], [15], [17]. This also allows all of the modulators to be formed from a single lamination stack. Fig. 4 illustrates the impacts of the modulator bridge thickness and position. The bridge provides a flux leakage path, so increasing its thickness reduces the slip torque. This is exacerbated if the bridge is placed near the outer air gap because Rotor 3's higher pole count produces shorter leakage paths and more leakage flux. Nonetheless, the impact of the bridge position is less significant for this design than it is in [5] because this design has a lower gear ratio, so there is less difference between the pole counts on Rotors 1 and 3. The reduction in slip torque as the bridge gets thicker reduces the efficiency when operating at maximum torque. The loss distribution is also affected. As the bridge thickness increases, the losses in both sets of PMs decrease for two reasons. First, the bridge reduces the spatial harmonics in the modulators' permeance function. Second, it short-circuits some of the flux, especially higher spatial harmonics, preventing these harmonics from crossing both air gaps and causing eddy currents in the PMs. However, a thicker bridge increases core losses in Rotor 2 due to the losses in the heavily saturated bridge itself. As specified in Table I and shown in Fig 5, this prototype design has a 1.5 mm thick bridge on the inner edge of Rotor 2.

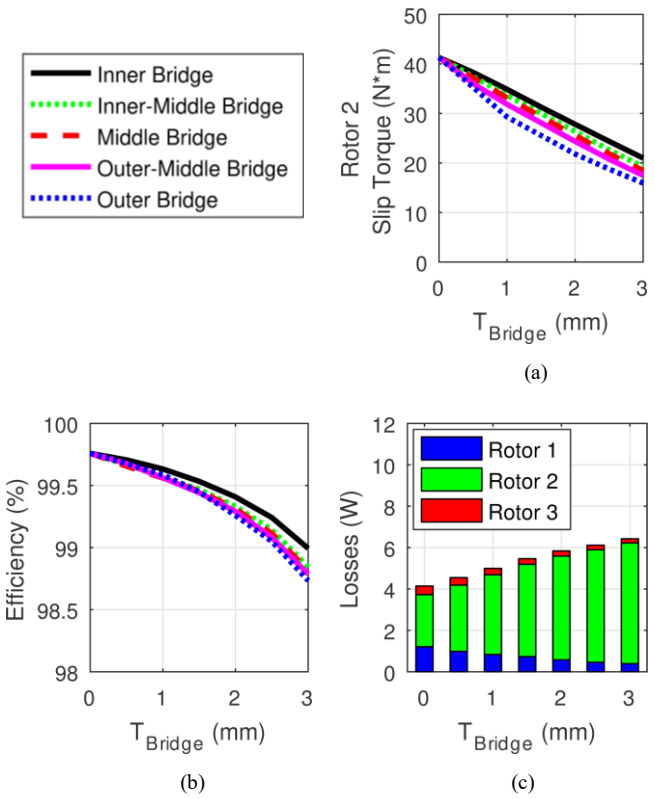

Fig. 4. Impact of the modulator bridge position and thickness on (a) 3D FEA Rotor 2 slip torque and (b) 2D FEA electromagnetic efficiency at rated speed and maximum torque. (c) Impact of the modulator bridge thickness with the bridge at the inner edge of Rotor 2 on the 2D FEA loss distribution at rated speed.

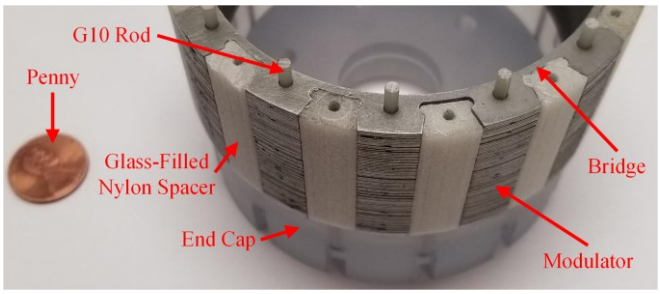

Fig. 5. The prototype's modulators affixed to one of the end caps with a penny for a size reference.

Fig. 5 shows the prototype's modulators with the spacers and rods inserted and one of the end caps attached. In addition to the rods connecting the modulators to the end caps, the end caps were affixed to the spacers with screws.

III. Magnet Retention

Retaining the PMs is another critical challenge. One conventional solution for machines is to fit a sleeve over the PMs, but this increases the effective air gaps. Fig. 6 illustrates the impacts of the effective air gaps on the performance of the design. As the air gaps increase, the slip torque decreases. The outer air gap has a larger impact on slip torque than the inner air gap because Rotor 3 has a higher pole count than Rotor 1, which leads to more leakage flux in the outer air gap. Increasing either

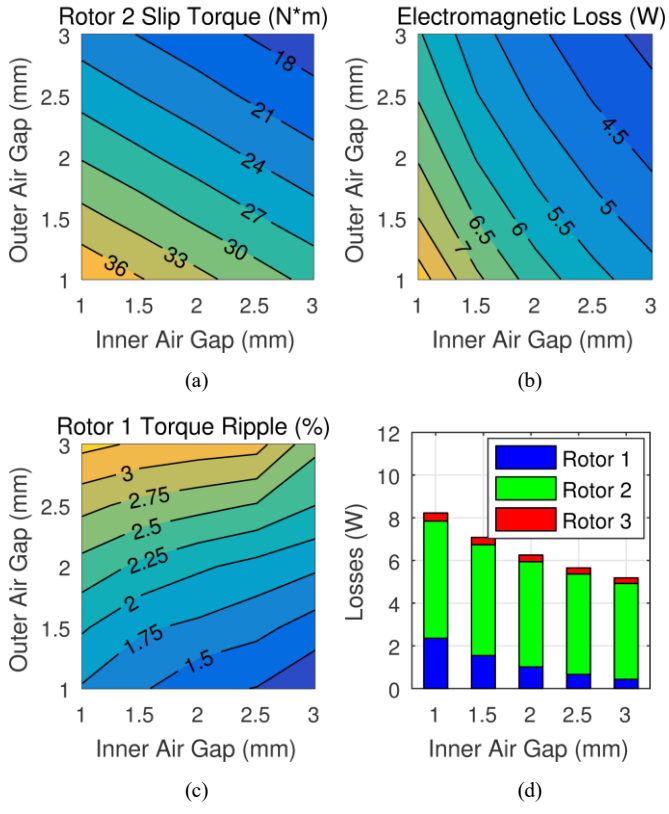

Fig. 6. Impact of the effective air gaps on (a) 3D FEA Rotor 2 slip torque, (b) 2D FEA electromagnetic losses at rated speed and maximum torque, and (c) Rotor 1 peak-to-peak torque ripple as a percentage of its slip torque. (d) Impact of the effective inner air gap with the outer air gap fixed at 1 mm on the 2D FEA loss distribution at rated speed.

air gap within the considered range tends to reduce the losses, with the inner air gap having a larger impact on the Rotor 1 PM losses and the outer air gap having a larger impact on the Rotor 3 PM losses. This occurs because the larger air gap attenuates the spatial flux harmonics. This effect is most pronounced for the inner air gap and the Rotor 1 PM losses because the permeance harmonics and Rotor 3 PM flux harmonics, which cause losses in the Rotor 1 PMs, have higher spatial frequencies than the Rotor 1 PM flux harmonics, and a larger air gap has a more significant effect on higher frequency spatial harmonics. While increasing the inner air gap within this range does slightly increase the electromagnetic efficiency, increasing the outer air gap does not increase the efficiency because this also significantly reduces the slip torque and, thus, the transmitted power. Similarly, the reduction of these spatial harmonics with an increasing air gap decreases the torque ripple as the inner air gap increases. Despite the use of a relatively low Rotor 1 pole pair count of 3 to simplify the prototype fabrication, the non-integer gear ratio [5] and Halbach arrays [10], [11] also keep the torque ripple relatively small. This design has an outer air gap of 1 mm and an effective inner air gap of 2.5 mm, including a 1 mm physical air gap and a 1.5 mm thick sleeve made of a polycarbonate-like plastic called Accura 60. Accura 60 was used for the Rotor 1 and Rotor 3 cores and for all of the end caps.

In a conventional magnetic gear without Halbach arrays and with back irons, the Rotor 3 PMs are attracted to the Rotor 3 back iron. However, the Halbach array results in forces pushing the radially magnetized PMs inward towards Rotor 2. Thus, it is necessary to retain the Rotor 3 PMs, but it is highly undesirable to do this in a way that increases the effective magnetic air gap. One alternative is to reduce the PM fill factor and use nonmagnetic walls between the PMs to hold them in place, particularly if the walls are wider at the radial inside than they are at the outside, as shown in Fig. 2(a). On Rotor 1, adding walls between the magnets allows the sleeve to be formed as a single piece with the plastic core and strengthens the sleeve. For both rotors, these walls also help to position the PMs. Fig. 7 illustrates the impact of changing the widths of the walls between adjacent PMs. Comparing Fig. 6(a) and Fig. 7(b) reveals that reducing the Rotor 3 PM fill factors to accommodate this retention strategy lowers the slip torque less than increasing the effective outer air gap to insert a Rotor 3 PM retention sleeve. Furthermore, this has a negligible impact on the electromagnetic efficiency. This design uses nonmagnetic walls between the Rotor 3 PMs that are 1.5 mm wide at their inner radius and 2 mm wide at their outer radius. Additionally, uniform 1.5 mm wide nonmagnetic walls between the Rotor 1 PMs connect the Rotor 1 plastic core with the Rotor 1 PM retention sleeve. The widths chosen for this design were limited by the constraints of the additive manufacturing process.

In addition to using sleeves and walls to retain the PMs, the PMs can be extended axially beyond the modulators and retained by partial sleeves in the region axially beyond the modulators. As suggested in [15], decreasing the modulators' stack length so that it is slightly shorter than the PM axial lengths can increase the slip torque. Fig. 8 illustrates the impact of axially extending the Rotor 1 and Rotor 3 PMs beyond the modulators with the modulators stack length fixed at 37.8 mm. Fig. 8 shows that extending the Rotor 1 PMs increases the torque

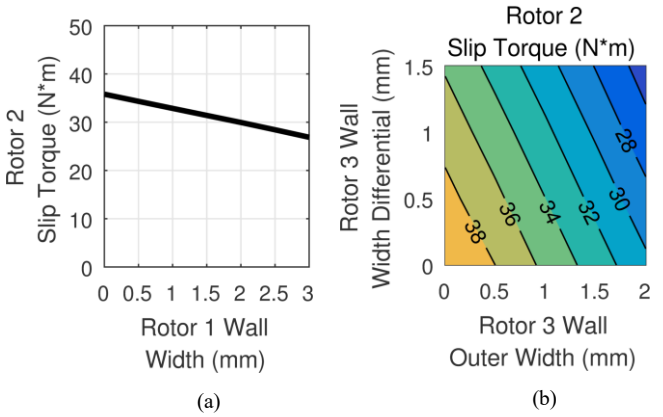

Fig. 7. (a) Impact of the wall width between the Rotor 1 PMs on the 3D FEA Rotor 2 slip torque. (b) Impact of the wall width and taper between the Rotor 3 PMs on the 3D FEA Rotor 2 slip torque.

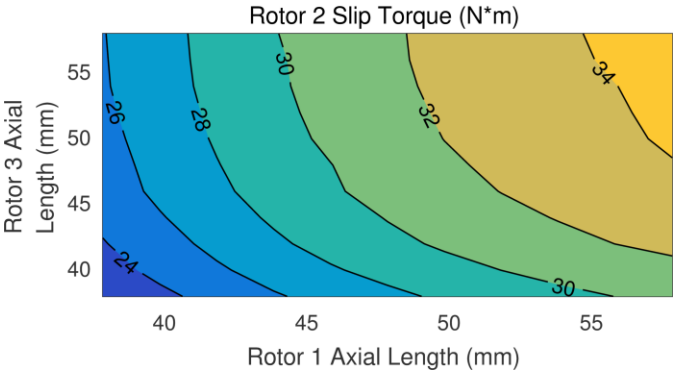

Fig. 8. Impact of the PM axial lengths on the 3D FEA Rotor 2 slip torque with the modulators' stack length fixed at 37.8 mm.

more than extending the Rotor 3 PMs the same amount. However, the Rotor 3 PMs can be extended several millimeters axially beyond the Rotor 1 PMs without increasing the gear's overall volume because the Rotor 3 end caps must extend axially beyond the Rotor 1 end caps. For this prototype, the axial lengths of the Rotor 1 and Rotor 3 PMs were selected as 47.8 mm and 51.8 mm, respectively. Fig. 9(a) shows part of a cross-section of the magnetically active portions of the design, and Figs. 9 (b)-(d) show the initial versions of the Rotor 3 and Rotor 1 plastic cores with the PMs inserted. However, when the PMs were inserted into the Rotor 1 plastic core, the outward forces on the radially magnetized PMs caused it to bulge outward by as much as 0.5 mm in some places. Therefore, a new Rotor 1 plastic core was designed with the radially magnetized Rotor 1 PMs moved inward by 0.5 mm, which reduced the simulated Rotor 2 slip torque from 31.1 N·m to 30.4 N·m. Additionally, the Rotor 1 plastic core was axially shortened and the Rotor 1 end cap was redesigned to interlock with the magnets to provide additional support. The redesigned Rotor 1 is shown in Fig. 9(e).

Additionally, a magnetically ideal version of the design was simulated with no holes in the modulators, no modulator bridge, 1 mm inner and outer air gaps, and 100% PM fill factors. 3D FEA predicted that this ideal design would have a Rotor 2 slip torque of 69.1 N·m. Thus, the very conservative choices made to facilitate the fabrication and assembly of this prototype reduced the slip torque by about 56%.

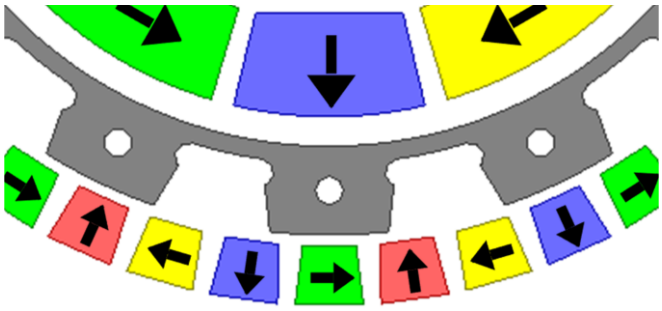

(a)

(b)

(c)

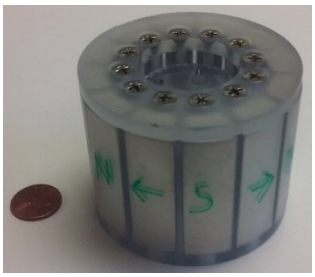

(d)

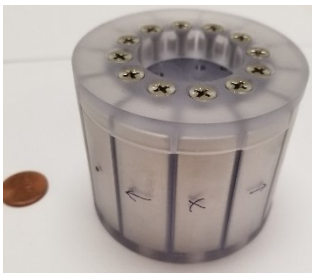

(e)

Fig. 9. (a) Model view of the magnetically active portions of the magnetic gear. Views of the Rotor 3 plastic core with PMs (b) with a penny for a size reference and (c) zoomed in on the PMs and walls. (d) The initial and (e) revised Rotor 1 plastic cores and end caps with PMs and a size reference penny.

IV. Impact of Back Irons

The prototype base design was also simulated with 5 mm thick back irons on both Rotors 1 and 3. Based on 3D FEA, this increases the Rotor 2 slip torque by 9%, but it also increases the design's magnetically active mass from 1.2 kg to 2.2 kg, which results in a net 40% reduction in the active gravimetric torque density (GTD). However, the back irons would provide two significant advantages. First, with plastic cores, the magnetic forces pulling the radially magnetized PMs into the air gaps can reach 330 N on the Rotor 1 PMs and 170 N on the Rotor 3 PMs, but, with back irons, the forces attracting the PMs to the back irons would be stronger than the magnetic forces pulling the PMs towards the air gap. Second, back irons would significantly improve flux containment, as shown in Fig. 10. Since the Halbach arrays have only two pieces per pole, they only provide a limited amount of flux shielding. Additionally, much of the flux beyond Rotor 3 comes from the Rotor 1 PMs [16], so much of this flux is not affected by using more pieces per pole on Rotor 3. Using a higher Rotor 1 pole pair count would shorten the paths of the flux produced by the Rotor 1 PMs and reduce the extent to which the Rotor 1 flux escapes beyond Rotor 3.

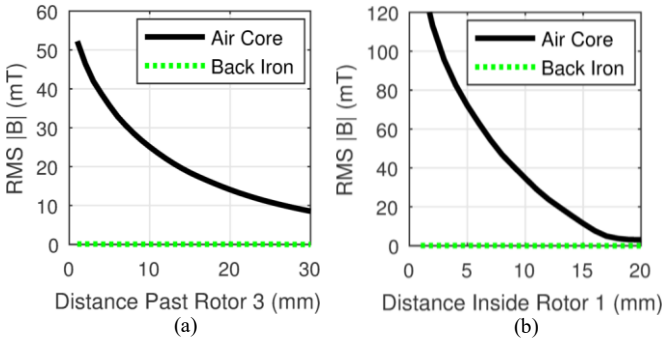

Fig. 10. Flux density at different radial distances (a) beyond a 5 mm thick Rotor 3 back iron or plastic Rotor 3 core and (b) inside of a 5 mm thick Rotor 1 back iron or plastic Rotor 1 core.

V. Assembly

The modulator laminations were stacked and bonded. There was a secure fit between the modulator lamination stack and the G10 rods and the glass-filled nylon spacers. The rods and the screw holes in the spacers aligned well with the corresponding holes in the two end caps. Fig. 5 shows the resulting assembly with one of the end caps attached.

Tooling was created using additive manufacturing to facilitate safe insertion of the PMs. Fig. 11 illustrates the tooling for inserting the Rotor 1 PMs. This enabled the PMs to be aligned axially beyond most of the magnetic fields and then pushed into place. Similar tooling was created for inserting the Rotor 3 PMs. Also, the radially magnetized PMs were inserted before the tangentially magnetized PMs to avoid strong forces pushing the PMs being inserted away from the plastic cores. With this strategy, all of the PMs were successfully inserted, and each of the authors still has 10 unmaimed fingers. Fig. 9 shows the resulting assemblies.

The finished prototype is illustrated in Fig. 2(b). End supports were included to mount the prototype to the testbed. The overall mass of the prototype was 4.4 kg with the end supports and 3.6 kg without the end supports. Table II provides a breakdown of the measured masses of some of the different prototype components.

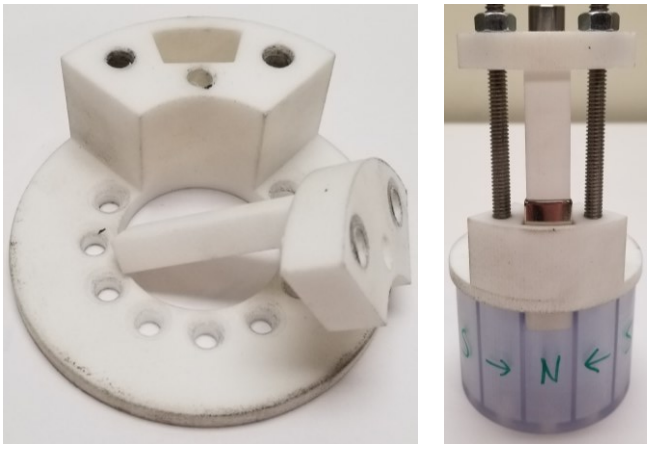

(a) (b)

Fig. 11. (a) Rotor 1 PM insertion tooling and (b) the Rotor 1 PM insertion tooling being used to insert a PM into Rotor 1.

TABLE II. PROTOTYPE MASS BREAKDOWN

	Mass (grams)
Rotor 1 PMs	480
Rotor 3 PMs	440
Modulator Laminations	320
Modulator Spacers and Rods	40
Rotor 1 Plastic Core and End Cap	130
Rotor 3 Plastic Core and End Cap	960
Modulator End Caps	190
Shafts	610
Bearings	180
Fasteners	240
End Supports	780

VI. EXPERIMENTAL RESULTS

The measured Rotor 2 slip torque was 31.2 N·m, which is 2.6% higher than the simulated slip torque of 30.4 N·m. This yields GTD values of 25.2 N·m/kg considering only the active material, 8.7 N·m/kg considering the total mass of the prototype without end supports, and 7.1 N·m/kg considering the total mass of the prototype with end supports. Significant improvements in GTD could be achieved by optimizing the usage of the structural material, especially if a stronger material, such as G10, were used for the plastic cores and end caps. However, the use of G10 would prevent the same additive manufacturing processes from being used.

Fig. 12 shows the experimental setup used to measure the prototype's losses under load. The PM machine was used as a motor to drive the high speed shaft of the prototype, and the induction machine was used as a generator to provide a mechanical load connected to the prototype's low speed shaft. Torque meters measured the torques on both shafts. The prototype was run up to 1800 rpm on the high speed shaft and 386 rpm on the low speed shaft. Fig. 13 shows that the measured speeds agree with the ideal 4.67:1 gear ratio. Fig. 14 compares the simulated electromagnetic no load losses with the measured no load losses. Fig. 15 compares the simulated electromagnetic losses and the measured losses under load, and Fig. 16 shows the measured efficiencies. In Figs. 15 and 16, the Rotor 2 torques are given as per unit values relative to Rotor 2's slip torque. While the measured losses are significantly higher than the simulated electromagnetic losses at higher speeds, likely due to mechanical losses, manufacturing tolerances, and experimental measurement precision limitations, the prototype is still extremely efficient, exceeding an efficiency of 99% at many operating points. This high efficiency makes it difficult to precisely measure the losses, so the results displayed in Figs. 14, 15(b), and 16 show some measurement noise. Because the losses do not vary much with the load torque and primarily vary with speed, the prototype achieves the highest efficiencies at high torques and low speeds.

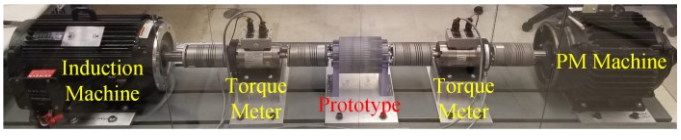

Fig. 12. Experimental test setup.

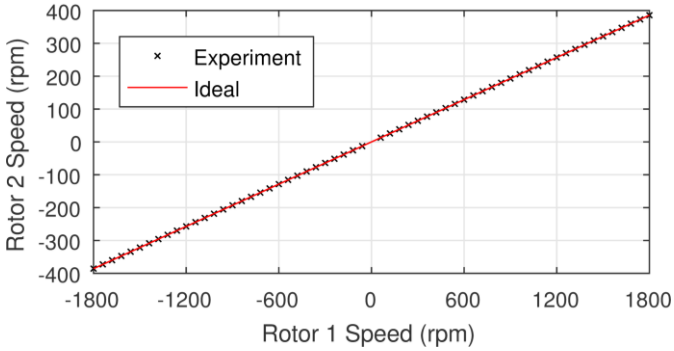

Fig. 13. Measured rotor speeds compared with the ideal 4.67:1 gear ratio.

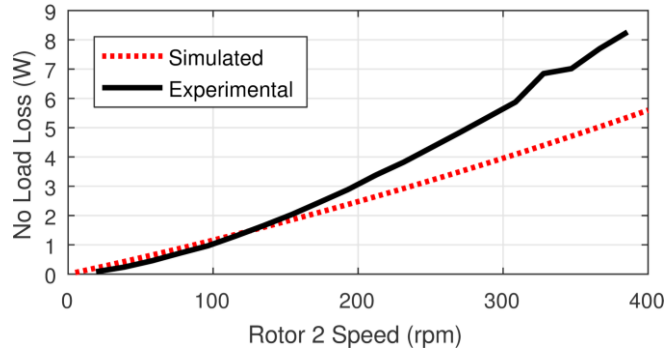

Fig. 14. Simulated electromagnetic and measured no load losses for the prototype.

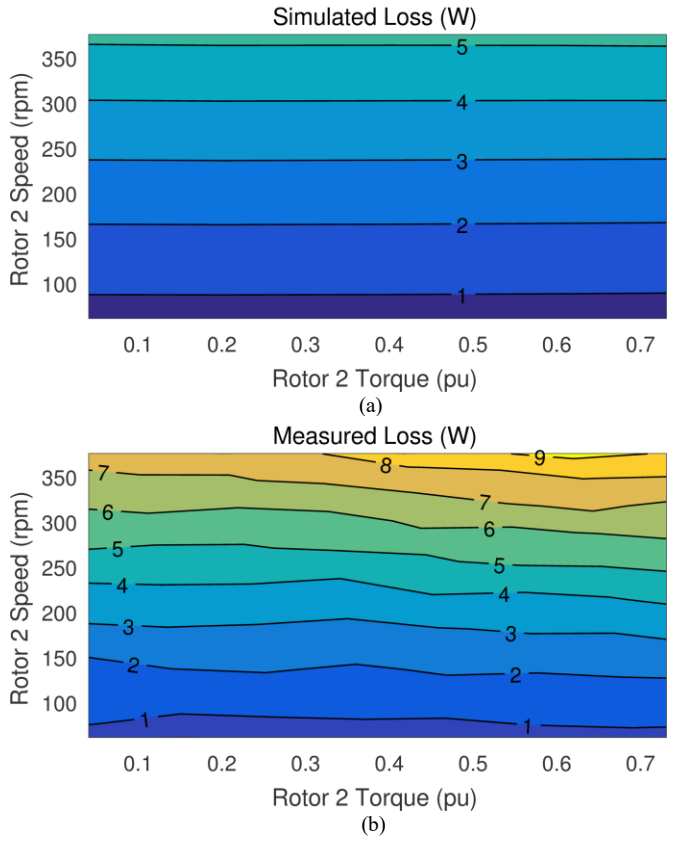

Fig. 15. (a) Simulated electromagnetic and (b) measured losses for the prototype under different load and speed operating conditions.

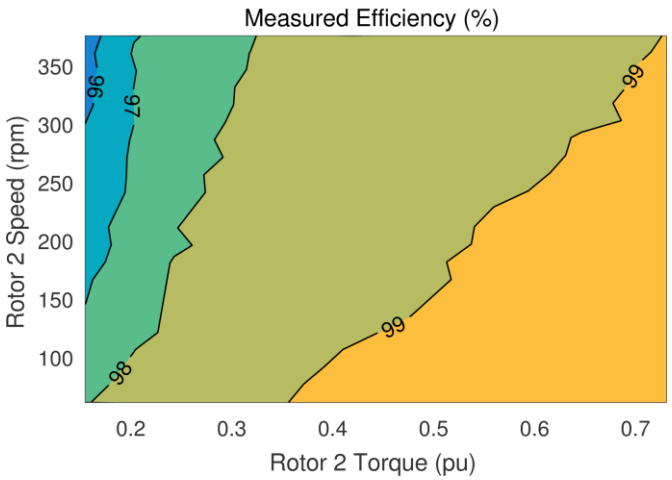

Fig. 16. Experimentally measured efficiency for the prototype under different load and speed operating conditions.

VII. Comparison with Mechanical Gears

Table III provides a comparison between the prototype and some similarly rated commercially available mechanical gears. The rated output torque and GTD listed for the prototype in Table III are based on the measured slip torque of the gear. However, most applications would likely require these values to be derated by some amount based on the effective inertia ratio of the system and how suddenly the torques on each side are changed [23]. Whereas mechanical gears are derated by an application-dependent service factor to extend their longevity, magnetic gears must be derated to avoid slipping based on the loads expected for a given application. Nonetheless, even if the magnetic gear's torque is rated at only 75% of the slip torque, the prototype still achieves an efficiency of approximately 99%.

Table III reveals significant variations in the performances of different commercially available mechanical gears. The example planetary gears achieve much higher efficiencies and GTDs than the example worm and helical gears. Additionally, for both the worm gear and planetary gear topologies, Table III illustrates a tradeoff between maximizing GTD and maximizing efficiency.

The prototype achieves a GTD that is comparable to the range of GTDs of the example worm and helical gears, but the prototype's GTD is significantly lower than the GTDs of the example planetary gears. However, the prototype's efficiency is higher than the nominal efficiency of any of the example mechanical gears.

VIII. Conclusion

Various options for securing the magnetically active portions of a magnetic gear with air cores and Halbach arrays were simulated.

- Circular cuts were made in the modulators to accommodate G10 rods and glass-filled nylon spacers. This enabled a good connection between the modulators and their end caps without a significant reduction in the gear's slip torque.
- A bridge was used to connect the modulators. This simplified the assembly process because the modulators could be formed as a single stack of laminations. However, the bridge significantly reduced the slip torque. This reduction was minimized by placing the bridge on the inner edge of the modulators.
- PM retention sleeves were evaluated for Rotors 1 and 3. However, increasing the effective air gaps due to the sleeves significantly reduced the slip torque, especially for the outer air gap. Therefore, a sleeve was only used on Rotor 1.
- Nonmagnetic walls were added between adjacent PMs on Rotors 1 and 3 to facilitate PM placement and retention. However, these walls significantly reduced the slip torque because they reduced the size of the PMs.
- The PMs were extended axially beyond the modulators so that the PMs could be retained by end caps in the space axially beyond the modulators. This increased the slip torque at the expense of increased mass and volume.

A prototype with a gear ratio of 4.67:1 and a Rotor 2 slip torque of 31.2 N·m was fabricated and tested. The prototype achieves GTDs of 25.2 N·m/kg when considering only the mass of the PMs and modulators, 8.7 N·m/kg when considering the total mass without the end supports, and 7.1 N·m/kg when considering the total mass including the end supports. While the active material GTD of 25.2 N·m/kg is competitive with the GTDs of the example commercial mechanical planetary gears listed in Table III, when the structural mass of the prototype is considered, the prototype's GTD becomes more comparable to those of the example commercially available worm and helical gears. However, the prototype's efficiency exceeds 99% at

TABLE III. Gear Comparison

Model Number	EL-B813-5-L	RS-RT 40	EPL-SA-064-5	PLPE070-005	CHC 20 PB 4,6	Prototype
Manufacturer	Grove Gear	Varvel	Eisele	Neugart	Chiaravalli	N/A
Gear Type	Worm	Worm	Planetary	Planetary	Helical	Magnetic
Gear Ratio	5:1	5:1	5:1	5:1	4.6:1	4.67:1
Rated Output Torque (N·m)	23.6	32.0	26.0	30.0	33.0	31.2
Rated Output Speed (rpm)	350	720	700	900	302	400
Nominal Efficiency	93%	89%	94%	97%	95%	99%
Mass (kg)	5.0	2.5	1.0	1.5	4.7	4.4
GTD (N·m/kg)	4.7	12.8	26.0	20.0	7.0	7.1
Reference	[18]	[19]	[20]	[21]	[22]	N/A

many operating points, which is higher than the nominal efficiencies of the example mechanical gears.

While this prototype did not achieve a GTD as high as that of some commercially available mechanical planetary gears, this analysis shows significant opportunities for improvement. Sacrifices made to facilitate assembly and to hold the various magnetically active components in place reduced the slip torque by about 56%. Eliminating the modulator bridge and relying only on the spacers between modulators and rods through the modulators would significantly increase the design's torque capacity. Additionally, if the PMs are only supported axially beyond the modulators, this would eliminate the torque penalties associated with retention sleeves and walls between adjacent PMs. Furthermore, the mass of the structural material, especially the additive manufacturing parts, could be significantly reduced.

ACKNOWLEDGMENT

Portions of this research were conducted with the advanced computing resources provided by Texas A&M High Performance Research Computing.

The authors would like to thank ANSYS for their generous support of the EMPE lab through the provision of FEA software.

REFERENCES

[1] K. Atallah and D. Howe, "A novel high-performance magnetic gear," *IEEE Trans. Magn.*, vol. 37, no. 4, pp. 2844–2846, Jul. 2001.

[2] P. O. Rasmussen, T. O. Anderson, F. T. Jorgensen, and O. Nielsen, "Development of a high performance magnetic gear," *IEEE Trans. Ind. Appl.*, vol. 41, no. 3, pp. 764-770, May-Jun. 2005.

[3] P. M. Tlali, R.-J. Wang, and S. Gerber, "Magnetic gear technologies: A review," in *Proc. Int. Conf. Elect. Mach.*, 2014, pp. 544–550.

[4] L. Jian, K. T. Chau, and J. Z. Jiang, "A magnetic-geared outer-rotor permanent-magnet brushless machine for wind power generation," *IEEE Trans. Ind. Appl.*, vol. 45, no. 3, pp. 954-962, May-Jun. 2009.

[5] M. Johnson, M. C. Gardner, H. A. Toliyat, S. Englebretson, W. Ouyang, and C. Tschida, "Design, construction, and analysis of a large scale inner stator radial flux magnetically geared generator for wave energy conversion," *IEEE Trans. Ind. Appl.*, vol. 54, no. 4, pp. 3305-3314 Jul.-Aug. 2018.

[6] H. Baninajar, J. Z. Bird, S. Modaresahmadi and W. Williams, "Electromagnetic and mechanical design of a hermetically sealed magnetic gear for a marine hydrokinetic generator," in *Proc. IEEE Energy Convers. Congr. and Expo.*, 2018, pp. 4987-4993.

[7] T. V. Frandsen, L. Mathe, N. I. Berg, R. K. Holm, T. N. Matzen, P. O. Rasmussen, and K. K. Jensen, "Motor integrated permanent magnet gear in a battery electrical vehicle," *IEEE Trans. Ind. Appl.*, vol. 51, no. 2, pp. 1516–1525, Mar.-Apr. 2015.

[8] J. J. Scheidler, V. M. Asnani and T. F. Tallerico, "NASA's magnetic gearing research for electrified aircraft propulsion," in *Proc. AIAA/IEEE Elect. Aircraft Technol. Symp.*, 2018, pp. 1-12.

[9] R. S. Dragan, R. Clark, E. K. Hussain, K. Atallah and M. Odavic, "Magnetically geared pseudo direct drive for safety critical applications," *IEEE Trans. Ind. Appl.*, vol. 55, no. 2, pp. 1239-1249, Mar.-Apr. 2018.

[10] L. Jian and K. T. Chau, "A coaxial magnetic gear with Halbach permanent-magnet arrays," *IEEE Trans. Energy Convers.*, vol. 25, no. 2, pp. 319-328, Jun. 2010.

[11] M. Johnson, M. C. Gardner, and H. A. Toliyat, "Analysis of axial field magnetic gears with Halbach arrays," in *Proc. IEEE Int. Elect. and Mach. Drives Conf.*, 2015, pp. 108-114.

[12] A. Rahideh, A. A. Vahaj, M. Mardaneh, and T. Lubin, "Two-dimensional analytical investigation of the parameters and the effects of magnetisation patterns on the performance of coaxial magnetic gears," *IET Elec. Syst. Transp.*, vol. 7, no. 3, pp. 230-245, Aug. 2017.

[13] L. Jian, K. T. Chau, Y. Gong, J. Z. Jiang, C. Yu and W. Li, "Comparison of coaxial magnetic gears with different topologies," *IEEE Trans. Magn.*, vol. 45, no. 10, pp. 4526-4529, Oct. 2009.

[14] K. K. Uppalapati and J. Z. Bird, "An iterative magnetomechanical deflection model for a magnetic gear," *IEEE Trans. Magn.*, vol. 50, no. 2, pp. 245-248, Feb. 2014.

[15] H. Y. Wong, J. Z. Bird, D. Barnett, and W. Williams, "A high torque density Halbach rotor coaxial magnetic gear," in *Proc. IEEE Int. Elect. and Mach. Drives Conf.*, 2019, pp. 233-239.

[16] M. C. Gardner, D. A. Janak and H. A. Toliyat, "A parameterized linear magnetic equivalent circuit for air core radial flux coaxial magnetic gears with Halbach arrays," in *Proc. IEEE Energy Convers. Congr. and Expo.*, 2018, pp. 2351-2358.

[17] S. Gerber and R-J. Wang, "Analysis of the end-effects in magnetic gears and magnetically geared machines," in *Proc. IEEE Int. Conf. Elect. Mach.*, 2014, pp. 396-402.

[18] Grove Gear, "Electra-Gear EL series eCatalog," [Online]. Available: http://grovegear.smartcats.com/ecatalog/Electragear-EL-Single-Solid/en/EL-B813-5-L. Accessed: Jun. 13, 2019.

[19] Varvel, "RS RT catalog," [Online]. Available: http://www.varvel.com/varvel-download/3248. Accessed: Jun. 13, 2019.

[20] Eisele Getriebe, "Eisele katalog planetengetriebe," [Online]. Available: http://eisele-getriebe.com/wordpress/wp-content/uploads/2017/03/Eisele-Katalog_Planetengetriebe_20170312.pdf. Accessed: Jun. 13, 2019.

[21] Neugart, "Product catalog: PLPE," [Online]. Available: https://static.neugart.com/fileadmin/user_upload/Downloads/Catalog_Chapters/Neugart_PLPE_EN.pdf. Accessed: Jun. 13, 2019.

[22] Chiaravalli, "Gear boxes and motors catalog," [Online]. Available: https://feyc.eu/download/catalogos/transmision/chiaravalli/Gear%20Boxes%20and%20Motors%20%20(1).pdf. Accessed: Jun. 13, 2019.

[23] M. C. Gardner and H. A. Toliyat, "Nonlinear analysis of magnetic gear dynamics using superposition and conservation of energy," in *Proc. IEEE Int. Elect. Mach. and Drives Conf.*, 2019, pp 210-217.